Microwave-Assisted Synthesis of Pt/Graphene Nanocomposites for Nonenzymatic Hydrogen Peroxide Sensor

Fengyuan Zhang, Zaihua Wang, Yuzhen Zhang, Zhixiang Zheng, Chunming Wang[*], Yongling Du, Weichun Ye

Department of Chemistry, Lanzhou University, Lanzhou 730000, P.R. China,
[*]E-mail: wangcm@lzu.edu.cn

A sensitive nonenzymatic hydrogen peroxide (H_2O_2) sensor was fabricated based on Pt/graphene (Pt/GN) nanocomposites. The nanocomposites were rapidly synthesized via a one-step microwave-assisted method, and characterized by X-ray diffraction, transmission electron microscopy, and X-ray photoelectron spectroscopy. The results exhibited that Pt nanoparticles (NPs) were well-dispersed on the graphene surface with the average diameter of about 3.2 nm. Cyclic voltammetry results demonstrated that the Pt/GN nanocomposites modified glassy carbon electrode (Pt/GN/GCE) exhibited excellent electrocatalytic activity to the reduction of H_2O_2. Amperometric response results indicated that Pt/GN/GCE displayed a fast response of less than 4 s with linear range of 2.5-6650 μM and a relatively low detection limit of 0.8 μM (S/N = 3). In addition, the Pt/GN/GCE showed good selectivity for H_2O_2 detection in the presence of several interfering species under physiological pH condition.

Keywords: Graphene; Pt nanoparticle; microwave; nonenzymatic; hydrogen peroxide sensor

1. INTRODUCTION

The reliable, accurate and rapid determination of hydrogen peroxide (H_2O_2) has received considerable attention in recently years because H_2O_2 plays a significant role in many fields including clinic, food, pharmaceutical and environmental analyses [1]. Therefore, many analytical methods such as spectrometry [2], chemiluminescence [3] and electrochemistry [4–6] have been used to detect H_2O_2. Among these analytical techniques, enzyme- and non-enzymatic based electrochemical sensors have attracted considerable interest due to its high sensitivity, fast response, low cost and convenient operation [7-10]. Compared with enzymatic sensors, nonenzymatic H_2O_2 sensors based on functional nanocomposites have several advantages such as high stability, easy handling and wide responding

range [11, 12]. Actually, many efforts have been paid to develop non-enzymatic sensors, for instance, electrodes modified with ZnO nanorod arrays [13], MnO_2-modified vertically aligned multi-walled carbon nanotubes [14], Se/Pt nanocomposites [15] and Pt nanoparticles/ordered mesoporous carbon nanocomposite [16]. Although these materials exhibited electrocatalytic activities towards the electrochemical redox reaction of H_2O_2, novel electrode materials with high sensitivity and good selectivity are still highly desirable in this field.

Recently, Graphene nanosheets (GN) has received considerable interest in electrochemistry filed due to its high surface areas (calculated value, 2630 m^2/g), low cost, and super conductivity (10^3-10^4 S/m) [17-19]. In addition, the decoration of graphene with metal nanoparticles (NPs) could provide larger electrochemically active surface areas for the adsorption of biomolecules and effectively accelerate the electron transfer between electrode and detection molecules, which could lead to a more rapid and sensitive current response [20]. Up to now, there have been some reports of electrochemical sensor based on GN-metal nanocomposites, for instance, Ag nanoparticles/graphene nanosheet composites as H_2O_2 sensor [21], Pt/ionic liquid/graphene nanocomposite as ascorbic acid and dopamine sensor [22] and graphene-Pt nanoparticle hybrid material as cholesterol biosensor [23]. However, to the best of our knowledge, there are few paper reported the application of Pt and graphene nanocomposite in H_2O_2 sensing.

In this work, a nonenzymatic H_2O_2 sensor was fabricated based on Pt/graphene (Pt/GN) nanocomposites, which was synthesized by a rapid one-step microwave-assisted approach. The Pt NPs are uniform in particle size and are well-dispersed on the grapheme surface. The Pt/GN hybrids modified glassy carbon electrode (GCE) has a larger current to the reduction of H_2O_2 than the single-component Pt NPs. So it can be used to determine H_2O_2 with a low detection limit and a wide linear range.

2. EXPERIMENTAL

2.1. Chemicals and Apparatus

Graphite flake (nature,-325 mesh) was purchased from Alfa Aesar. H_2PtCl_6 was purchased from Tianjin Chemical Factory (Tianjin, China). Ascorbic acid (AA) and acetaminophen (AP) were purchased from Sigma. H_2O_2 (30%), glucose, sucrose, citric acid and urea were purchased from Sinopharm Chemical Reagent Co., Ltd. All other chemicals were purchased from Beijing Chemical Reagent Factory (Beijing, China) and were of analytical grade. 0.1 M phosphate buffer solution (PBS, pH=7.4) was prepared with 0.1 M Na_2HPO_4 and 0.1 M NaH_2PO_4. All solutions were prepared with doubly distilled water, purified by the Milli-Q system (Millipore Inc., 18.2 MΩ cm). Graphene oxide (GO) was prepared from graphite powder by a modified Hummers method [24].

Electrochemical measurements were performed on a CHI 660A electrochemical workstation (Shanghai Chenhua, China) with a three-electrode system consisting of an saturated calomel electrode (SCE) as the reference electrode, a platinum wire electrode as the auxiliary electrode and a bare or modified GCE (Φ=3 mm) as the working electrode. The morphology of the samples was characterized

using high resolution transmission electron microscopy (HRTEM, Tecnai G2 F30, FEI, USA). The phase structures of the samples were determined by X-ray diffraction (XRD) using a D/Max 2400 Rigaku diffractometer with Cu-Kα radiation (k = 0.15418 nm). X-ray photoelectron spectroscopy (XPS) was performed on a VG ESCA LAB 210 electron spectrometer using an Mg-Kα line excitation source with the reference of C1s at 285.0 eV. The microwave reactions were performed using a Galanz WD800ASL23-3 microwave oven (Guangzhou Galanz Co.Ltd., Guangzhou, China).

2.2. Synthesis of Pt/Graphene nanocomposites

In a typical synthesis, 10 mL of 1 mg/mL GO ethylene glycol (EG) solution was added into 9 mL of water, followed by the addition of 1 mL of 0.1 M H_2PtCl_6 aqueous solution. After being immediately ultrasonically treated for 1 h to ensure GO being uniformly dispersed in EG–water solution, the solution was placed for microwave oven for 120 s (power: 1040 W) and then cooled naturally to the room temperature (Scheme 1). The mixture was filtrated and washed copiously with water for several times to remove the remaining EG, and then dried in a vacuum desiccator at room temperature. The resulting product was labeled as Pt/GN. For comparison, Pt NPs and GN were also achieved by the same procedure.
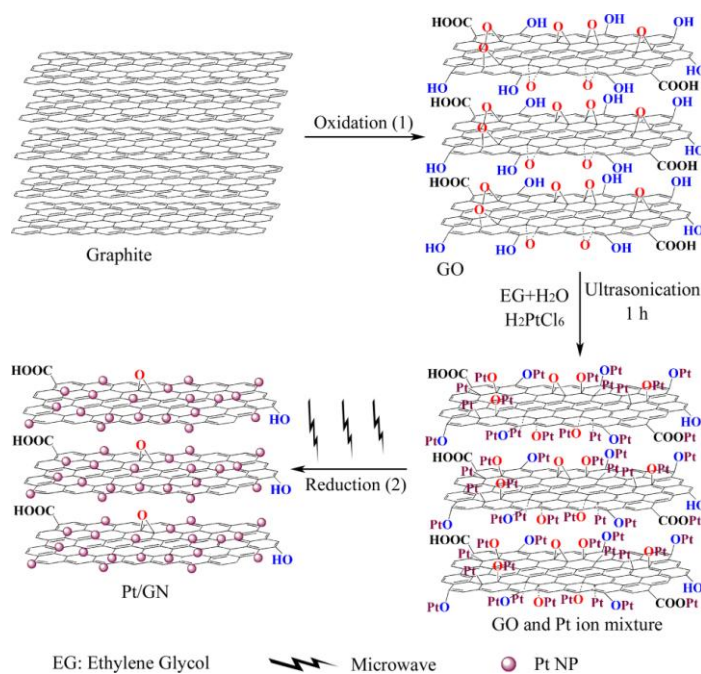
Scheme 1. Scheme shows a formation route to anchor Pt nanoparticles onto GN. (1) Oxidation of pure graphite powder to GO. (2) Formation of Pt/GN hybrids.

2.3. Fabrication of electrochemical sensor

Before modification, the GCE was first polished with 0.3 and 0.05 µm alumina slurry, and sonicated in ethanol and water successively. For the preparation of Pt/GN/GCE, 2.5 µL of 2.0 mg ml^{-1}

dimethylformamide-nafion (49:1 volume ratio) solution was dropped on the pretreated GCE and dried in a desiccator. For comparison, GN/GCE and Pt/GCE were also prepared by the same procedure. The electrolyte solutions were deoxygenated with N_2 and kept under N_2 atmosphere during electrochemical examinations.

3. RESULTS AND DISCUSSION

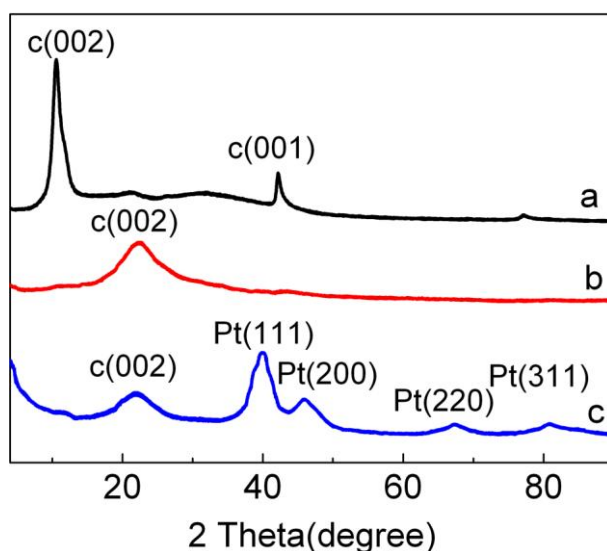*3.1 Characteristics of the Pt/GN nanocomposites*

Figure 1. XRD spectrums: (a) GO; (b) GN; (c) Pt/GN.

The phase structures of the samples were examined by XRD measurements, Figure 1 shows the XRD patterns of GO, GN and Pt/GN. It is clearly seen in Figure 1a that the typical diffraction peak (002) of GO locates at 10.6°, which is ascribed to the introduction of various oxygenic functional groups (epoxy, hydroxyl, carboxyl and carbonyl) attached on both sides and edges of carbon sheets. These oxygen-containing functional groups will subsequently serve as locating sites for metal complexes [25]. In Figure 1b, the typical diffraction peak (002) of GN shifts to higher angle ($2\theta=21.2°$). This is due to the partial removal of the oxygen-containing functional groups during reduction process, which means the partially reduction of GO sheets to GN and restacked into an ordered crystalline structure. Figure 1c shows the XRD of Pt/GN. The strong diffraction peaks at $2\theta=39.7°$, 46.0°, 67.4° and 80.1° are in good agreement with the (111), (200), (220) and (311) crystal planes of pure Pt with face-centered-cubic (fcc) phase (JCPDS 87-0647), respectively. It can be seen in Figure 1c that the position of the (002) diffraction peak ($2\theta=21.7°$) moves slightly to higher angle after deposition of Pt NPs on graphene surface, which indicates that GO is further converted to the crystalline graphene, and the conjugated graphene network (sp2 carbon) has been reestablished due to the reduction process [26].
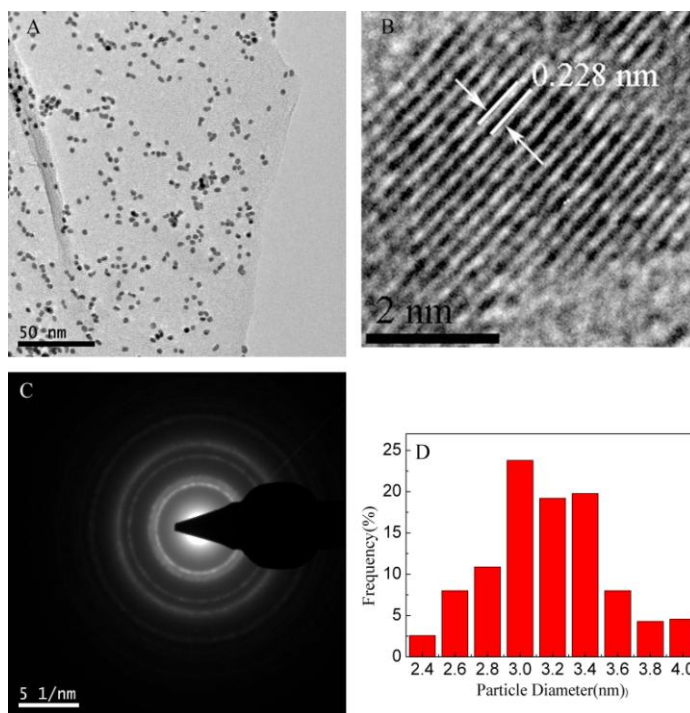
Figure 2. (A) TEM image of Pt/GN, (B) HRTEM image of Pt NPs in Pt/GN hybrids, (C) SAED pattern of Pt, (D) Histogram of Pt particle size distribution.
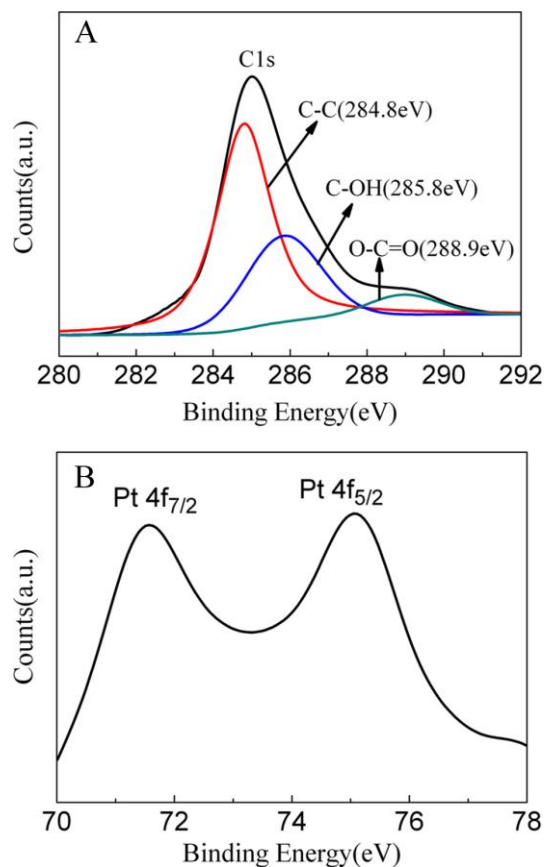

Figure 3. XPS spectra of Pt/GN: (A) C1s, (B) Pt 4f.

Morphology of Pt/GN nanocomposites has been characterized by TEM. It is clearly seen in Figure 2A that Pt NPs were uniformly distributed on transparent graphene surface and no particles scattered out of the support, indicating a strong interaction between graphene support and particles. Highly dispersed Pt NPs on support with larger surface areas has advantages in catalytic activity and sensor sensitivity [27]. Therefore, Pt/GN hybrids should be a potential material for use in future nanotechnology. The high resolution image of Pt/GN hybrids in Figure 2B shows the oriented and ordered lattice fringes for Pt NPs. The d-spacing value of 0.228 nm coincides with that of fcc Pt (111). The ring-like selected-area electron diffraction (SAED) pattern indicates that the as-synthesized Pt NPs are polycrystalline structures (Figure 2C). The histogram of particle size distribution (Figure 2D) shows that Pt NPs on graphene surface have a narrow size distribution and the average diameter was about 3.2 nm.

In addition, we employed the XPS measurements to further determine the Pt/GN hybrids. The C1s spectrum shows peaks at 284.8, 285.8, and 289.0 eV, which correspond to C-C, C-OH, and O-C=O chemical binding states, respectively (Figure 3A). These observations indicated that GO isn't completely reduced into graphene with a spot of oxygen-containing functional groups during reduction process. This conclusion is consistent with the XRD result. Figure 3B shows the XPS spectrum of Pt, it is found that two obvious peaks at 71.6 and 75.1 eV can be easily observed, assigning to the Pt $4f_{7/2}$ and $4f_{5/2}$.

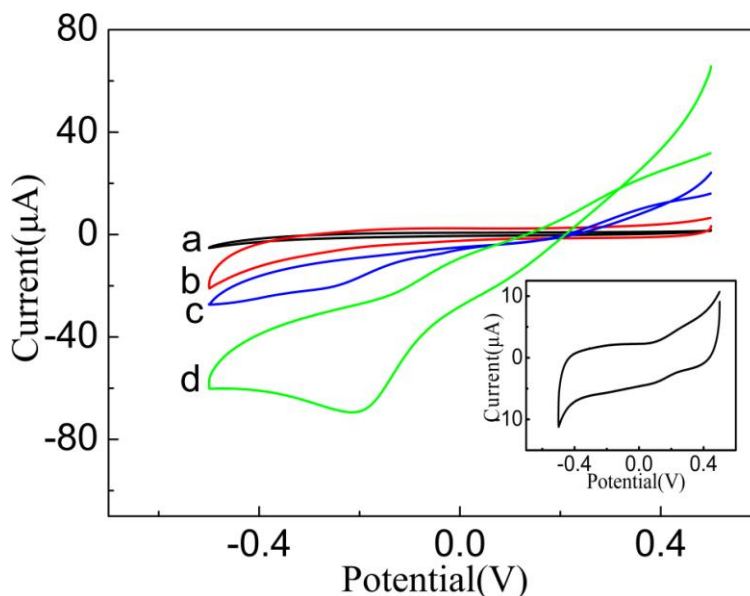*3.2 Electrochemical performances of the Pt/GN/GCE towards H_2O_2*

Figure 4. CVs of (a) bare GCE, (b) GN/GCE, (c) Pt/GCE, and (d) Pt/GN/GCE in 0.1 M PBS (pH=7.4) containing 5 mM H_2O_2 at 20 mV·s^{-1}. Inset: the CV of Pt/GN/GCE in 0.1 M phosphate buffer solution (pH=7.4) without H_2O_2.

Figure 4 shows cyclic voltammetry (CV) responses of 5.0 mM H_2O_2 in 0.1 M PBS (pH=7.4) at different electrodes. No redox peaks are observed in the absence of H_2O_2 for Pt/GN/GCE (Inset of

Figure 4), indicating that the modified electrode is non-electroactive in the selected potential region. After injecting 5 mM H_2O_2 into the PBS, no reduction peak is observed on bare GCE (curve a) and GN/GCE (curve b), which interprets that H_2O_2 reduction could not be achieved at bare GCE and GN/GCE. For Pt/GN/GCE, a remarkable reduction peak at about -0.216 V is observed (curve d), which is 40 mV positively shifted compared with that of Pt/GCE (curve c). Moreover, the reduction peak current on Pt/GN/GCE is thrice as that on Pt/GCE. The more positive peak potential and higher reductive current clearly suggest that the Pt/GN exhibits much better electrocatalytic ability towards H_2O_2 than Pt NPs. This improved electrocatalytic ability could be attributed to the synergistic effect of Pt NPs and GN, in which Pt NPs has electrocatalytic ability towards H_2O_2 and the GN provides a large specific surface area to increase the loading amount of H_2O_2. On the other hand, GN acts as a good support for achieving a high dispersion of Pt NPs, preventing them from serious aggregation and thus preserving the high catalytic performance of Pt NPs [20].

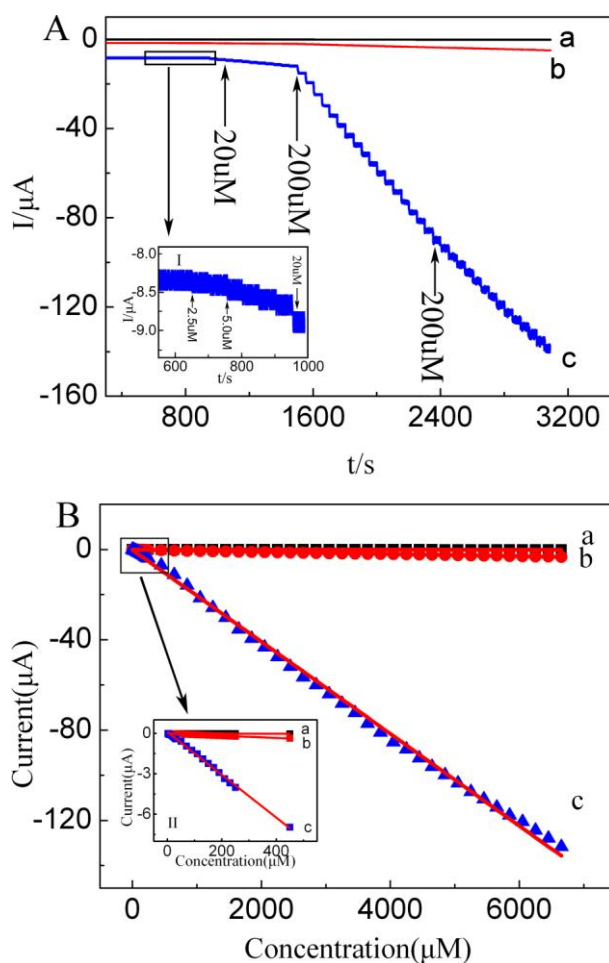*3.3 Amperometric response and calibration curve for H_2O_2 detection*

Figure 5. (A) I-t response curve for successive injection of H_2O_2 at (a) GN/GCE, (b) Pt/GCE and (c) Pt/GN/GCE, measured at -0.20 V. Inset I: magnified image of the region in the rectangle. (B) Calibration curves of response current versus H_2O_2 concentration on (a) GN/GCE, (b) Pt/GCE and (c) Pt/GN/GCE. Inset II: magnified image of the region in the rectangle.

Table 1. Comparison of the performance of various hydrogen peroxide sensors.

Electrode materials	Potential applied (V)	Linear range (μM)	Detection limit (μM)	Reference
Se/Pt nanocomposites	0(vs. SCE)	10-15000	3.1	15
Pt nanoparticles/ordered mesoporous carbon nanocomposite	-0.1(vs.Ag/AgCl)	2-4212	1.2	16
Pt nanoparticle-loaded carbon nanofiber electrode	0(vs. Ag/AgCl)	1-800	0.6	28
Pt/polypyrrole hybrid hollow microspheres	-0.1(vs. Ag/AgCl)	1000-8000	1.2	29
Gold nanowire	-0.2(vs. Ag/AgCl)	1.2-800	1.2	30
Hemoglobin/Laponite/Chitosn	-0.25(vs. SCE)	6.2-2550	6.2	31
Au–graphene–HRP–chitosan biocomposites	-0.3(vs. Ag/AgCl)	5-5130	1.7	32
Mesoporous Platinum Microelectrodes	0.6 (vs. SCE)	20-40000	4.5	33
Pt/graphene nanocomposite	-0.20(vs. SCE)	2.5-6650	0.8	This work

Figure 5A shows the typical I–t curve of these modified electrodes with successive injection of H_2O_2 at the potential of -0.20 V. As can be seen Pt/GN/GCE could achieve the maximum steady-state current within 4 s after the injection of H_2O_2 (curve c). However, no obvious response or weak signal is obtained on the GN/GCE (curve a) and Pt/GCE (curve b), respectively. The corresponding current-concentration calibration plots in Figure 5B clear show that the Pt/GN/GCE (curve c) displays a remarkable sensitivity compared with that of GN/GCE (curve a) and Pt/GCE (curve b). The high sensitivity is mainly due to the super conductivity of the composite and the large active surface area of Pt/GN. For Pt/GN/GCE, a linear relationship is established in the range of 2.5 μM to 6650 μM with a detection limit of 0.8 μM based on a signal-to-noise ratio (S/N) of 3. The regression equation is $I(\mu A) = -0.0204 C_{H_2O_2} - 0.1106$ with a correlation coefficient of 0.9986. A comparison of linear range, detection limit, and detection potential for Pt/GN/GCE with other H_2O_2 sensors reported in the literature is shown in Table 1. All the data reveal the analytical parameters for Pt/GN/GCE are comparable and even better than those obtained at several electrodes reported recently. Therefore, the Pt/GN nanocomposites are a good electrode material for preparation of low detection potential, sensitive, and wide linear range amperometric sensor for H_2O_2.

3.4 Interference study

For evaluating selectivity of the Pt/GN nanocomposites modified electrode, various possible interfering species were examined for their effect on the determination of H_2O_2. As shown in Figure 6, the response current of AA, AP, glucose, sucrose, citric acid and urea do not cause any observable interference to the determination of H_2O_2. This suggests that these species had no obvious interference in the reduction of H_2O_2.
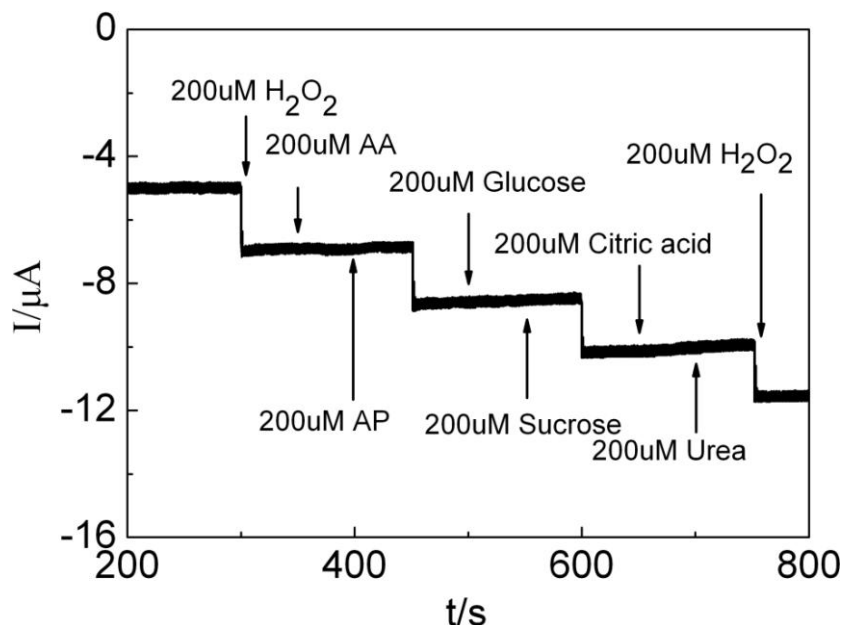
Figure 6. I-t response curve of the Pt/GN/GCE upon successive addition of 200 μM H_2O_2, AA, AP, glucose, sucrose, citric acid and urea in 0.1 M PBS (pH=7.4) at -0.20V.

3.5 Stability and reproducibility

Besides sensitivity and selectivity, the reproducibility of the Pt/GN nanocomposites modified electrode was also investigated. The relative standard deviation (RSD) of current signal for 200 μM H_2O_2 was 3.98% for 12 measurements for the same electrode at -0.20 V. The RSD for 6 modified electrodes prepared at the same conditions was 4.60%. When the Pt/GN/GCE was stored at room temperature for one week, the current response to 200 μM H_2O_2 remained 91.8% of its original value, suggesting the long-term stability of the electrode.

4. CONCLUSIONS

Pt/GN nanocomposites have been prepared via a facile one-step microwave-assisted method and could be used to fabricate a novel nonenzymatic sensor for the detection of H_2O_2. The electrochemical results showed that the Pt/GN/GCE exhibited high sensitivity, good selectivity, wide linear range and low detection limit for amperometric detection of H_2O_2. Therefore, the Pt/GN nanocomposites provide a promising platform for the study of the application of graphene nanocomposites in electrocatalysis and the construction of attractive nonenzymatic amperometric sensor in the future.

References

1. S.J. Yao, J.H. Xu, Y. Wang, X.X. Chen, Y.X. Xu, S.S. Hu, *Anal. Chim. Acta* 557 (2006) 78.
2. C. Matsubara, N. Kawamoto, K. Takamura, *Analyst* 117 (1992) 1781.
3. K. Nakashima, K. Maki, S. Kawaguchi, S. Tsukamoto, I. Kazuhiro, *Anal. Sci.* 7 (1991) 709.
4. K. Cui, Y.H. Song, Y. Yao, Z.Z. Huang, L. Wang, *Electrochem. Commun.* 10 (2008) 663.
5. S.M. Golabi, J.B. Raoof, *J. Electroanal. Chem.* 416 (1996) 75.
6. Y.H. Song, L. Wang, C.B. Ren, G.Y. Zhu, Z. Li, *Sens. Actuators B* 114 (2006) 1001.
7. S.Y. Xu, B. Peng, X.Z. Han, *Biosens. Bioelectron.* 22 (2007) 1807.
8. Y.Y. Wang, X.J. Chen, J.J. Zhu, *Electrochem. Commun.* 11 (2009) 323.
9. N.N. Wei, X. Xin, J.Y. Du, J.L. Li, *Biosens. Bioelectron.* 26 (2011) 3602.
10. C.M. Welch, C.E. Banks, A.O. Simm, R.G. Compton, *Anal. Bioanal. Chem.* 382 (2005) 12.
11. A.I. López-Lorente, B.M. Simonet, M. Valcárcel, *Anal. Bioanal. Chem.* 399 (2011) 43.
12. C. Batchelor-McAule y, Y. Du, G.G. Wildgoose, R.G. Compton, *Sens. Actuators B: Chem.* 135 (2008) 230.
13. J. Wang, M.Z. Xu, R.G. Zhao, G.N. Chen, *Analyst* 135 (2010) 1992.
14. B. Xu, M.l. Ye, Y.X. Yu, W.D. Zhang, *Anal. Chim. Acta* 674 (2010) 20.
15. Y. Li, J.J. Zhang, J. Xuan, L.P. Jiang, J.J. Zhu, *Electrochem. Commun.* 12 (2010)777.
16. X.J. Bo, J.C. Ndamanisha, J. Bai, L.P. Guo, *Talanta* 82 (2010) 85.
17. S.J. Guo, S.J. Dong, E.K. Wang, *ACS Nano* 4(2010) 547.
18. H.L. Guo, X.F. Wang, Q.Y. Qian, F.B. Wang, X.H. Xia, *ACS Nano* 3 (2009) 2653.
19. S. Stankovich, D.A. Dikin, R.D. Piner, K A. Kohlhaas, A. Kleinhammes, Y.Y. Jia,Y. Wu, S.T. Nguyen, R.S. Ruoff, *Carbon* 45 (2007) 1558.
20. M. Pumera, *Chem. Soc. Rev.* 39 (2010) 4146.
21. S. Liu, J.Q. Tian, L. Wang, X.P. Sun, *J. Nanopart. Res.* 13 (2011) 4539.
22. F.H. Li, J. Chai, H.F. Yang, D.X. Han, L. Niu, *Talanta* 81 (2010) 1063.
23. R.S. Dey, C.R. Raj, *J. Phys. Chem.* C 114 (2010) 21427.
24. S. Gilje, S. Han, M.S. Wang, K.L. Wang, R.B Kaner, *Nano Lett* 7 (2007) 3394.
25. C.C. Chien, K.T. Jeng, *Mater Chem Phys* 99 (2006) 80.
26. Y.J. Li, W. Gao, L.J. Ci, C.M. Wang, *Carbon* 48 (2010) 1124.
27. Y.C. Xing, *J. Phys. Chem. B* 108 (2004) 19255.
28. Y. Liu, D.W. Wang, L. Xu, H.Q. Hou, T.Y. You, *Biosens. Bioelectron.* 26(2011)4585.
29. X.J. Bian, X.F. Lu, E. Jin, L.R. Kong, W.J. Zhang, C. Wang, *Talanta* 81 (2010) 813.
30. S.J. Guo, D. Wen, S.J. Dong, E.K. Wang, *Talanta* 77(2009) 1510.
31. D. Shan, E. Han, H.G. Xue, S. Cosnier, *Biomacromolecules* 8 (2007) 3041.
32. K.F. Zhou, Y.H. Zhu, X.L. Yang, J. Luo, C.Z. Li, S.R. Luan, *Electrochim. Acta* 55 (2010) 3055.
33. S.A.G. Evans, J.M. Elliott, L.M. Andrews, P.N. Bartlett, P.J. Doyle, G. Denuault, *Anal. Chem.* 74 (2002) 1322.